Inorganic Chemistry

Article

pubs.acs.org/IC

Metal–Ligand Synergistic Effects in the Complex Ni(η^2-TEMPO)$_2$: Synthesis, Structures, and Reactivity

Derek Isrow,[†] Nathan J. DeYonker,[‡] Anjaneyulu Koppaka,[†] Perry J. Pellechia,[§] Charles Edwin Webster,*[,‡] and Burjor Captain*[,†]

[†] Department of Chemistry, University of Miami, Coral Gables, Florida 33124, United States

[‡] Department of Chemistry, The University of Memphis, Memphis, Tennessee 38152, United States

[§] Department of Chemistry and Biochemistry, University of South Carolina, Columbia, South Carolina 29208, United States

Supporting Information

ABSTRACT: In the current investigation, reactions of the "bow-tie" Ni(η^2-TEMPO)$_2$ complex with an assortment of donor ligands have been characterized experimentally and computationally. While the Ni(η^2-TEMPO)$_2$ complex has *trans*-disposed TEMPO ligands, proton transfer from the C–H bond of alkyne substrates (phenylacetylene, acetylene, trimethylsilyl acetylene, and 1,4-diethynylbenzene) produce *cis*-disposed ligands of the form Ni(η^2-TEMPO)(κ^1-TEMPOH)(κ^1-R). In the case of 1,4-diethynylbenzene, a two-stage reaction occurs. The initial product Ni(η^2-TEMPO)-(κ^1-TEMPOH)[κ^1-CC(C_6H_4)CCH] is formed first but can react further with another equivalent of Ni(η^2-TEMPO)$_2$ to form the bridged complex Ni(η^2-TEMPO)(κ^1-TEMPOH)[κ^1-κ^1-CC(C_6H_4)CC]Ni(η^2-TEMPO)(κ^1-TEMPOH). The corresponding reaction with acetylene, which could conceivably also yield a bridging complex, does not occur. Via density functional theory (DFT), addition mechanisms are proposed in order to rationalize thermodynamic and kinetic selectivity. Computations have also been used to probe the relative thermodynamic stabilities of the *cis* and *trans* addition products and are in accord with experimental results. Based upon the computational results and the geometry of the experimentally observed product, a *trans*–*cis* isomerization must occur.

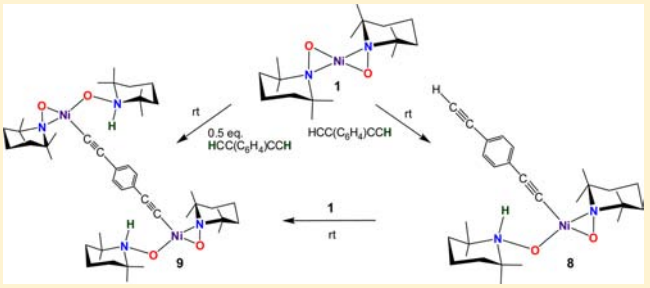

INTRODUCTION

Since its discovery in 1960, the stable radical 2,2,6,6-tetramethylpiperidine-*N*-oxide (TEMPO)[1] has been shown to be a valuable tool in the fields of radical polymerization,[2] oxidation reactions, and catalysis,[3] as well as in electron spin resonance (ESR) studies utilizing nitroxide spin probes.[4] The coordination chemistry of this paramagnetic species has also been shown to afford complexes adopting both η^1 and η^2 bonding motifs.[5]

Lately, a few metal-TEMPO complexes exhibiting both catalytic and stoichiometric reactions have garnered much visibility.[6] For example, a recent report shows the elimination of NO gas from a Ni-bipy complex upon reaction with TEMPO.[6d] Stahl has shown that a (bipy)Cu^I/TEMPO catalyst system with NMI (bpy = 2,2′-bipyridine, NMI = *N*-methylimidazole) is an efficient catalyst for the aerobic oxidation of alcohols to aldehydes and ketones, which rivals the activity and selectivity of palladium catalytic systems.[6a,b] In another example, an Fe-TEMPO complex has been investigated for the oxidation of 9,10-dihydroanthraquinone and also primary and secondary alcohols, with a mechanism involving proton atom transfer from the organic substrate to the nitrogen atom of the κ^1-coordinated TEMPO ligand.[6c] A recent report also shows the oxygen atom transfer capability of an Fe-TEMPO complex, which leads to formation of an Fe(III) oxo intermediate.[6h]

We recently reported the preparation of the complex Ni(η^2-TEMPO)$_2$ (**1**), which contains exclusively TEMPO ligands.[7] Subsequent reactions of complex **1** with donor ligands such as *tert*-butyl isocyanide and phenylacetylene proceeded in a facile manner to yield the complexes Ni(η^2-TEMPO)(η^1-TEMPO)-(κ^1-CN^{t}Bu) (**2**) and Ni(η^2-TEMPO)(κ^1-TEMPOH)(κ^1-CCPh) (**3**). The reactivity of complex **1** is assisted by the TEMPO ligand to transform from an η^2 binding mode to an η^1 binding mode. Furthermore, the formation of **3** was surprising, as this reaction included proton transfer from phenyl acetylene to a coordinated TEMPO ligand. Herein, we report that **1** also reacts with other donor ligands, including pyridine, acetylene, trimethylsilyl acetylene, and 1,4-diethynylbenzene, as depicted in Scheme 1.

EXPERIMENTAL SECTION

General Data. Unless indicated otherwise, all reactions were performed under an atmosphere of argon. Reagent-grade solvents were dried by the standard procedures and were freshly distilled prior to use. Solution-phase infrared spectra were recorded on a Nicolet 380

Received: May 23, 2013
Published: November 21, 2013

Scheme 1

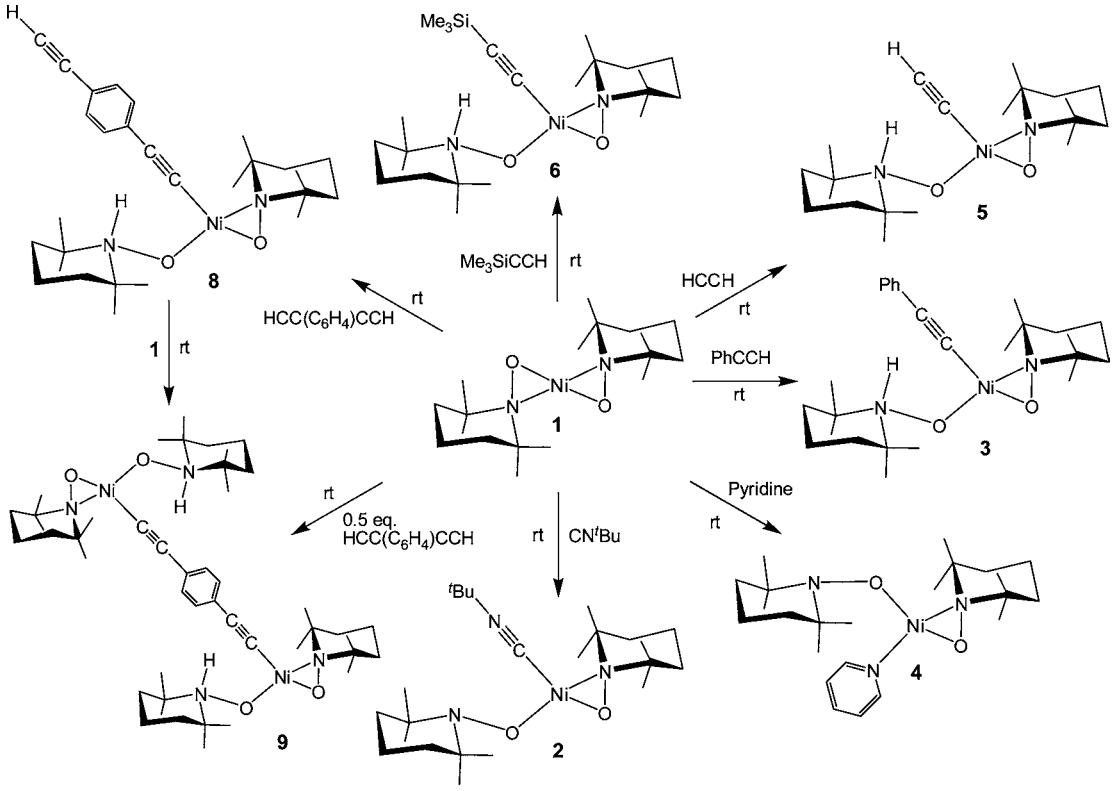

FT-IR spectrophotometer. Single-crystal FTIR spectra were obtained on a Perkin−Elmer Spectrum 400 using a Perkin−Elmer Universal ATR Sampling Accessory. ^{1}H NMR spectra were recorded on a Bruker 400 spectrometer operating at 399.993 MHz. 2D [^{1}H, ^{15}N] HSQC NMR were collected on a Bruker Avance-IIIHD 500 NMR spectrometer operating at 500.21 MHz for ^{1}H and 50.69 MHz for ^{15}N at the University of South Carolina. Elemental analyses were performed by Columbia Analytical Services (Tucson, AZ). Electrospray mass spectrometric measurements were obtained on a Bruker micrOTOF-Q II. Bis(1,5-cyclooctadiene)nickel, Ni(COD)$_2$, was purchased from Strem Chemicals, used without further purification, and stored and handled in a drybox. TEMPO (2,2,6,6-tetramethylpiperidine-*N*-oxide), *tert*-butyl isocyanide, and phenylacetylene were purchased from Alfa Aesar and used without further purification. 1,4-Diethynylbenzene was purchased from TCI and used without further purification. Atomic-absorption-grade acetylene and argon (UHP grade) were purchased from AirGas and used without further purification. Phenylacetylene-d_1 (99%), pyridine, and trimethylsilyl acetylene were purchased from Sigma−Aldrich and used without further purification. The syntheses of Ni(η^2-TEMPO)$_2$, (complex **1**), Ni(η^2-TEMPO)(η^1-TEMPO)(κ^1-CN^{t}Bu), (complex **2**), and Ni(η^2-TEMPO)(κ^1-TEMPOH)(κ^1-CCPh), (complex **3**) have been previously described,[7] but have been slightly modified under further investigation.

Synthesis of Ni(η^2-TEMPO)$_2$ (1). A 100 mg (0.36 mmol) amount of Ni(COD)$_2$ and 115 mg (0.72 mmol) of TEMPO were loaded into a Schlenk flask. Thirty milliliters (30 mL) of hexane solvent was then added to the flask using a cannula. The stirred solution changed color from light orange to deep purple as it was heated to reflux, for ∼5 min. The solvent was then removed in vacuo, and the residue was dissolved in 4 mL of diethyl ether, filtered into a glass vial, and placed in a −25 °C freezer in a drybox. Evaporation of solvent afforded 105 mg (78% yield) of purple crystalline blocks of Ni(η^2-TEMPO)$_2$. Spectral data for **1**: ^{1}H NMR (C_6D_6 in ppm): δ = 2.39 (s, 12 H, 4 CH_3), 1.36 (s, 12 H, 4 CH_3), 1.40−1.25 (m, broad, 12 H, 6 CH_2). Mass spectroscopy ES$^+$/MS calculated for [M$^+$ + CH_3CN], 412; found 412. The isotope distribution is consistent with the presence of one Ni atom.

Synthesis of Ni(η^2-TEMPO)(η^1-TEMPO)(κ^1-CN^{t}Bu) (2). A 40 mg (0.108 mmol) amount of Ni(η^2- TEMPO)$_2$ was loaded into a side arm Schlenk flask and dissolved in 20 mL of hexane, after which 10 mg (0.125 mmol) of ^{t}BuNC was added, resulting in an immediate color change from purple to dark red. The reaction mixture was stirred at room temperature for 10 min. The volatiles were removed in vacuo and the residue was dissolved in 2 mL of diethyl ether, filtered into a glass vial, and placed in a −25 °C freezer in a drybox. Evaporation of solvent afforded 44 mg (90% yield) of red crystalline blocks of Ni(η^2-TEMPO)(η^1-TEMPO)(κ^1-CN^{t}Bu). Spectral data for **2**: IR ν_{CN} (cm^{-1}, in hexane) 2169. ^{1}H NMR (toluene-d_8 in ppm): δ = 2.46 (s), 2.43−1.00 (broad), 1.55 (s), 1.50−1.20 (broad), 1.19−1.02 (broad multiplet), 0.95 (s). Note: The ^{1}H NMR spectrum at room temperature indicates some dynamical processes in solution (see Figure S1 in the Supporting Information). Mass spectroscopy EI/MS: m/z calculated for M$^+$ = 453; found 453; calcd (M$^+$-^{t}BuNC) = 370 (= Ni(η^2-TEMPO)$_2$); found 370. The isotope distribution is consistent with the presence of one Ni atom.

Synthesis of Ni(η^2-TEMPO)(κ^1-TEMPOH)(κ^1-CCPh) (3). A 40 mg (0.108 mmol) amount of Ni(η^2-TEMPO)$_2$ was loaded into a side-arm Schlenk flask and dissolved in 20 mL of hexane. Twelve milligrams (12 mg) (0.117 mmol) of phenylacetylene was added and the reaction mixture was stirred at room temperature for 1 h, during which time the color changed from purple to light red. The volatiles were then removed in vacuo and the residue dissolved in 2 mL of diethyl ether, filtered into a glass vial, and placed in a −25 °C freezer in a drybox. Evaporation of solvent afforded 37 mg (73% yield) of red crystalline blocks of Ni(η^2-TEMPO)(κ^1-TEMPOH)(κ^1-CCPh). Spectral data for **3**: FTIR (single crystal) $\nu_{(C\equiv C)}$, 2079 (s) cm^{-1}; $\nu_{(N-H)}$, 3675−3100 (broad) cm^{-1}. FTIR $\nu_{(C\equiv C)}$ (cm^{-1} in hexane): 2074 (s). ^{1}H NMR (C_6D_6 in ppm): δ = 7.62 (s, 1 H, N−H), 7.50 (d, 2 H, Ph), 7.10 (t, 2 H, Ph), 6.96 (t, 1 H, Ph), 3.10 (s, 6 H, 2 CH_3), 2.11 (s, 6 H, 2 CH_3), 1.76 (br, 2 H, CH_2), 1.29 (s, 8 H, 2 CH_3 and 1 CH_2), 1.08 (m, 6 H, 3 CH_2), 0.90 (s, 8 H, 2 CH_3 and 1 CH_2). 2D [^{1}H, ^{15}N] HSQC NMR toluene-d_8, $^1J(^{15}N-H)$ = 78 Hz between atoms N2 and H1 (see Figure S2 in the Supporting Information). Mass spectroscopy ES$^+$/MS

dx.doi.org/10.1021/ic401296f | *Inorg. Chem.* 2013, 52, 13882−13893

calculated for $[M + H]^+$ = 473; found 473. The isotope distribution is consistent with the presence of one Ni atom.

*Synthesis of Ni(η^2-TEMPO)(η^1-TEMPO)(κ^1-NC_5H_5) (**4**).* A 40 mg (0.108 mmol) amount of Ni(η^2-TEMPO)$_2$ was loaded into a side-arm Schlenk flask and dissolved in 20 mL of hexane. Excess pyridine (0.1 mL) was added and the reaction mixture immediately changed color from purple to dark brown. The volatiles were then removed in vacuo and the residue dissolved in 2 mL of diethyl ether with a drop of pyridine, filtered into a glass vial, and placed in a −25 °C freezer in a drybox. Evaporation of solvent afforded 46 mg (95% yield) of brown blocks of Ni(η^2-TEMPO)(η^1-TEMPO)(κ^1-NC_5H_5). Spectral data for **4**: ^{1}H NMR (C_6D_6 in ppm, pyridine peaks and integrations not listed due to dynamical processes): δ = 2.96 (s), 2.35 (s), 3.0−1.8 (broad), 1.54 (s), 1.35 (s). ^{1}H NMR (NC_5D_5 in ppm, pyridine peaks and integrations not listed due to dynamical processes): δ = 3.03 (s), 2.38 (s), 3.0−1.8 (broad), 1.55 (s), 1.36 (s), 1.19 (s) (see Figure S3 in the Supporting Information). Mass spectroscopy ES$^+$/MS calculated for $[M]^+$ = 450 *m*/*z*; found 450 *m*/*z*. The isotope distribution is consistent with the presence of one Ni atom. It should be noted that additional peaks with higher molecular weights were also present in the mass spectrum, presumably because of decomposition in the spectrometer. Similarly, reliable elemental analysis results were not obtained for this relatively unstable compound.

*Synthesis of Ni(η^2-TEMPO)(κ^1-TEMPOH)(κ^1-CCH) (**5**).* A 40 mg (0.108 mmol) amount of Ni(η^2-TEMPO)$_2$ was loaded into a side-arm Schlenk flask and dissolved in 20 mL of hexane. Acetylene gas was purged through the reaction mixture and stirred at room temperature for 1 h, during which time the color changed from purple to light red. The volatiles were then removed in vacuo and the solid residue dissolved in 2 mL of diethyl ether, filtered into a glass vial, and placed in a −25 °C freezer in a drybox. Evaporation of solvent afforded 32 mg (74% yield) of red crystalline blocks of Ni(η^2-TEMPO)(κ^1-TEMPOH)(κ^1-CCH). Spectral data for **5**: FTIR $\nu_{(C\equiv C)}$ (cm^{-1} in hexane): 1933 (s). ^{1}H NMR (C_6D_6 in ppm): δ = 7.64 (s, 1 H, N−H), 3.10 (s, 6 H, 2 CH_3), 2.08 (s, 6 H, 2 CH_3), 2.06 (s, 1 H, CCH), 1.78 (m, 2 H, CH_2), 1.26 (s, 6 H, 2 CH_3), 0.90 (s, 6 H, 2 CH_3), 1.4−0.8 (m, broad, 10 H, 5 CH_2). Mass spectroscopy ES$^+$/MS calculated for $[M + H]^+$ = 397 *m*/*z*; found 397 *m*/*z*. The isotope distribution is consistent with the presence of one Ni atom.

*Synthesis of Ni(η^2-TEMPO)(κ^1-TEMPOH)(κ^1-$CCSiMe_3$) (**6**).* A 40 mg (0.108 mmol) amount of Ni(η^2-TEMPO)$_2$ was loaded into a side-arm Schlenk flask and dissolved in 20 mL of hexane. Twelve milligrams (12 mg) (0.122 mmol) of trimethylsilyl acetylene was added and the reaction mixture was stirred at room temperature for 1 h, during which time the color changed from purple to light red. The volatiles were then removed in vacuo and the residue dissolved in 2 mL of diethyl ether, filtered into a glass vial, and placed in a −25 °C freezer in a drybox. Evaporation of solvent afforded 40 mg (79% yield) of red crystalline blocks of Ni(η^2-TEMPO)(κ^1-TEMPOH)(κ^1-$CCSiMe_3$). Spectral data for **6**: FTIR $\nu_{(C\equiv C)}$ (cm^{-1} in hexane): 2009 (s). ^{1}H NMR (C_6D_6 in ppm): δ = 7.69 (s, 1 H, N−H), 2.99 (s, 6 H, 2 CH_3), 2.09 (s, 6 H, 2 CH_3), 1.76 (m, 2 H, CH_2), 1.26 (s, 6 H, 2 CH_3), 0.91 (s, 6 H, 2 CH_3), 1.5−0.9 (m, broad, 10 H, 5 CH_2), 0.29 (s, 9 H, $SiMe_3$). Mass spectroscopy ES$^+$/MS calculated for $[M + H]^+$ = 470 *m*/*z*; found 470 *m*/*z*. The isotope distribution is consistent with the presence of one Ni atom.

*Synthesis of Ni(η^2-TEMPO)(κ^1-TEMPOH)[κ^1-CC(C_6H_4)CCH] (**8**).* A 40 mg (0.108 mmol) amount of Ni(η^2-TEMPO)$_2$ was loaded into a side-arm Schlenk flask and dissolved in 20 mL of hexane. Fifteen milligrams (15 mg) (0.119 mmol) of 1,4-diethynylbenzene was added and the reaction mixture was stirred at room temperature for 1 h, during which time the color changed from purple to auburn red. The volatiles were then removed in vacuo and the residue dissolved in ∼2 mL of diethyl ether, filtered into a glass vial, and placed in a −25 °C freezer in a drybox. Evaporation of solvent afforded 27 mg (50% yield) of pure red crystalline blocks of Ni(η^2-TEMPO)(κ^1-TEMPOH)[κ^1-CC(C_6H_4)CCH]. Spectral data for **8**: FTIR $\nu_{(C\equiv C)}$ (cm^{-1} in CH_2Cl_2): 2071. ^{1}H NMR (C_6D_6): δ = 7.34 (s, 1 H, N−H), 7.40 (dd, 4 H, C_6H_4), 3.06 (s, 6 H, 2 CH_3), 2.77 (s, 1 H, C≡CH), 2.05 (s, 6 H, 2 CH_3), 1.70 (t, 2 H, 1 CH_2), 1.28 (s, 6 H, 2 CH_3), 1.20 − 1.35 (br, 4 H, 2 CH_2), 1.02−1.10 (br, 6 H, 3 CH_2), 0.88 (s, 6 H, 2 CH_3). Mass spectroscopy ES$^+$/MS calculated for $[M + H]^+$ = 497; found 497. The isotope distribution is consistent with the presence of one Ni atom.

*Synthesis of Ni(η^2-TEMPO)(κ^1-TEMPOH)[κ^1-κ^1-CC(C_6H_4)CC]Ni(η^2-TEMPO)(κ^1-TEMPOH) (**9**).* To 48 mg (0.129 mmol) of Ni(η^2-TEMPO)$_2$ and 8 mg (0.063 mmol) of 1,4-diethynylbenzene in a side-arm Schlenk flask, 20 mL of hexane was added. The reaction mixture was stirred at room temperature for 3 h, during which time the color changed from purple to auburn red. The volatiles were then removed in vacuo and the residue dissolved in ∼2 mL of benzene, filtered into a glass vial, and placed in a drybox. Evaporation of solvent at room temperature afforded 44 mg (80% yield) of pure red crystalline blocks of Ni(η^2-TEMPO)(κ^1-TEMPOH)[κ^1-κ^1-CC(C_6H_4)-CC]Ni(η^2-TEMPO)(κ^1-TEMPOH). Spectral data for **9**: FTIR $\nu_{(C\equiv C)}$ (cm^{-1} in hexane): 2073 (s). ^{1}H NMR (C_6D_6): δ = 7.66 (s, 2 H, N−H), 7.43 (s, 4 H, C_6H_4), 3.09 (s, 12 H, 4 CH_3), 2.10 (s, 12 H, 4CH_3), 1.73 (t, 4 H, 2 CH_2), 1.29 (s, 12 H, 4 CH_3), 1.20−1.36 (br, 8 H, 4 CH_2), 1.00−1.15 (br, 12 H, 6 CH_2), 0.90 (s, 12 H, 4 CH_3). Mass spectroscopy ES$^+$/MS calculated for $[M + H]^+$ = 868; found 868. The isotope distribution is consistent with the presence of two Ni atoms.

*Conversion of **8** to **9**.* To 20 mg (0.040 mmol) of **8** and 15 mg (0.040 mmol) of **1** in a side-arm Schlenk flask, 20 mL of hexane was added. The reaction mixture was stirred at room temperature for 2 h. The volatiles were then removed in vacuo and the residue dissolved in ∼2 mL of benzene, filtered into a glass vial, and placed in a drybox. Evaporation of solvent at room temperature afforded 22 mg (63% yield) of pure red crystalline blocks of **9**.

*Reaction of **1** with 6 equiv PhCCH and 6 equiv PhCCD.* To an equimolar mixture of PhCCH and PhCCD (44.4 μL, 0.404 mmol) dissolved in 0.6 mL of toluene-d_8 in a 5 mm NMR tube, 12.5 mg (0.034 mmol) of **1** was added. ^{1}H NMR after ∼10 min showed peaks corresponding to the product. Integration of the resonances indicated an ∼1:1 ratio for products **3** and **3**-d_1. Similarly, when the reaction was carried out in nondeuterated toluene solvent, ^{2}H{^{1}H} NMR showed two singlet resonances for the starting PhCCD and product **3**-d_1 with relative intensities of ∼1:11 (see Figures S5 and S6 in the Supporting Information).

*Reaction of **1** with Excess Pyridine.* A stock solution of **1** in C_6D_6 was prepared by dissolving 80.5 mg of **1** in 5 mL of C_6D_6. In an NMR tube, to 0.5 mL of this solution (0.022 mmol), 87 μL of pyridine (1.06 mmol) was added, followed by the addition of C_6D_6, such that the total volume was 1.023 mL. Similarly, in a series of experiments, to 0.5 mL solution of **1**, pyridine in the amounts of 174, 349, and 523 μL, was added. ^{1}H NMR spectra are shown in Figure S7 in the Supporting Information.

Crystallographic Analysis. Single crystals of **1**, **2**, **3**, **5**, **6**, and **8** suitable for X-ray diffraction (XRD) analysis were grown by evaporation of diethyl ether solutions at −25 °C. Single crystals of **4** suitable for XRD analysis were grown by evaporation of a diethyl ether solution with a drop of pyridine. Single crystals of **9** suitable for XRD analysis were grown by evaporation of a benzene solution. Data crystals for **5**, **6**, and **8** were glued to the end of a thin glass fiber for data collection under ambient conditions. Data crystals for **1**, **2**, **3**, **4**, and **9** were mounted onto the end of a thin glass fiber using Paratone-N for data collection at 100 K under flow of N_2. X-ray intensity data were measured using a Bruker SMART APEX2 CCD-based diffractometer using Mo Kα radiation (λ = 0.71073 Å).[8] The raw data frames were integrated with the SAINT+ program by using a narrow-frame integration algorithm.[8] Corrections for Lorentz and polarization effects were also applied with SAINT+. An empirical absorption correction based on the multiple measurement of equivalent reflections was applied using the program SADABS. All structures were solved by a combination of direct methods and difference Fourier syntheses, and refined by full-matrix least-squares on F^2, by using the SHELXTL software package.[9] All non-hydrogen atoms were refined with anisotropic displacement parameters. Hydrogen atoms were located from the difference map and refined with isotropic thermal parameters. Crystal data, data collection parameters, and results of the analyses are listed in Tables S1 and S2 in the Supporting Information.

dx.doi.org/10.1021/ic401296f | *Inorg. Chem.* 2013, 52, 13882−13893

Compounds Ni(η^2-TEMPO)$_2$ (**1**), Ni(η^2-TEMPO)(η^1-TEMPO)(κ^1-CN^{t}Bu) (**2**), Ni(η^2-TEMPO)(κ^1-TEMPOH)(κ^1-CCH) (**5**), Ni(η^2-TEMPO)(κ^1-TEMPOH)(κ^1-CCSiMe$_3$) (**6**), and Ni(η^2-TEMPO)(κ^1-TEMPOH)[κ^1-κ^1-CC(C_6H_4)CC]Ni(η^2-TEMPO)(κ^1-TEMPOH) (**9**) crystallized in the monoclinic crystal system. The systematic absences in the intensity data were consistent with the unique space group $P2_1/n$ for compounds **1** and **2**, and were consistent with the unique space group $P2_1/c$ for compounds **5**, **6**, and **9**. For compound **1**, with $Z = 2$, the molecule is crystallographically centrosymmetrical and thus contains only one-half of the formula equivalent of the molecule in the asymmetric crystal unit. For compound **9**, the molecule is also crystallographically centrosymmetrical, and, moreover, the asymmetric unit contains two molecules of benzene from the crystallization solvent that co-crystallized with the complex.

Compounds Ni(η^2-TEMPO)(κ^1-TEMPOH)(κ^1-CCPh) (**3**) and Ni(η^2-TEMPO)(κ^1-TEMPOH)[κ^1-*C*C(C_6H_4)CCH] (**8**) crystallized in the triclinic crystal system. The space group $P\bar{1}$ was assumed and confirmed by the successful solution and refinement of the structure. The compound Ni(η^2-TEMPO)(η^1-TEMPO)(κ^1-*N*C_5H_5) (**4**), crystallized in the orthorhombic crystal system. The systematic absences in the intensity data were consistent with the unique space group *Pbca*.

COMPUTATIONAL METHODS

All computations were performed using the Gaussian09 software package.[10] Gas-phase energies, optimized geometries, and unscaled harmonic vibrational frequencies were obtained using density functional theory (DFT).[11] The hybrid B3LYP[12] and pure PBEPBE[13] functionals were used with default grid parameters (the PBEPBE functional will be referred to as PBE throughout the article).[14] There are few qualitative differences between the structural and energetic PBE and B3LYP results. Therefore, all discussion in the text will refer to the PBE functional and B3LYP data will be presented as Supporting Information. The basis set for nickel was the Hay and Wadt basis set and effective core potential (ECP) combination (LANL2DZ),[15] as modified by Couty and Hall (Ni: 341/341/41),[16] where the two outermost p functions have been replaced by a split of the optimized Ni 4p function, respectively. All C, N, O, and H atoms utilized the 6-31G(d′) basis set.[17] Spherical harmonic d-functions were used throughout; i.e., there are five angular basis functions per d-function. The Hessian of the energy was computed at all stationary points to designate them as either minima or transition states (first-order saddle points). Zero-point energies (ZPE) and thermal enthalpy/free energy corrections were computed at 1 atm and 298.15 K. Aqueous solvation energies were computed using the SMD model with standard cavity parameters for *n*-hexane.[18] For the major reactants and products investigated, the computed singlet energies were generally lower by 8−10 kcal mol^{-1} than corresponding geometry-optimized triplet states. Therefore, all reported mechanisms and relative energies refer to closed-shell singlet species (except for the free TEMPO radical).

RESULTS AND DISCUSSION

As previously reported, the compound Ni(η^2-TEMPO)$_2$ (**1**) was afforded in 78% yield as the only nickel-containing product from the reaction of Ni(COD)$_2$ with TEMPO in hexane solvent at reflux (68 °C).[7] Complex **1** was characterized by NMR, mass spectrometry, and single-crystal X-ray diffraction analyses. An ORTEP depicting the molecular structure of **1** (also reported in ref 7) is shown (see Figure 1).

Once crystallographic complex number designations have been assigned in the discussion, they will henceforth be suffixed with a ***t*** or ***c*** to distinguish between the two isomeric possibilities (*trans* and *cis*) of the Ni(η^2-TEMPO)$_2$ complexes.

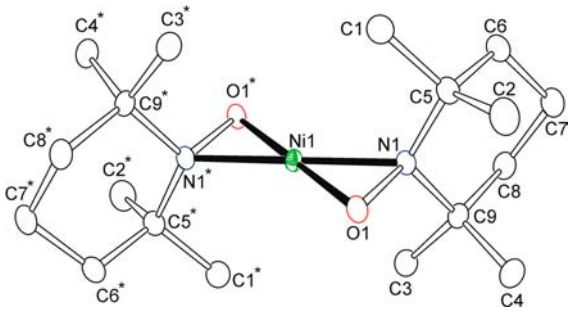

Figure 1. An ORTEP of the molecular structure of **1**, showing 50% thermal ellipsoid probability. Selected bond distances and angles are as follows: Ni1−O1 = 1.8404(11) Å, Ni1−N1 = 1.9360(10) Å, N1−O1 = 1.4136(12) Å, N1−C5 = 1.5240(16) Å, and N1−C5 = 1.5240(16) Å; O1−Ni1−O1* = 180.0°, N1−Ni1−N1* = 180.0°, N1−Ni1−O1 = 43.88(4)°, N1−Ni1−O1* = 136.12(4)°, N1−O1−Ni1 = 71.66(6)°, O1−N1−Ni1 = 64.47(6)°, C5−N1−O1 = 110.83(9)°, and C5−N1−Ni1 = 119.99(8)°.

Compound **1*t*** contains two TEMPO ligands that are η^2-coordinated to a Ni center. The Ni atom, along with the two N and O atoms, form a rectangular planar "bow-tie" type structure. In the solid state, the molecule lies about an inversion center and can be viewed to overall possess approximately C_{2h} symmetry. Bond angles and distances are consistent for an η^2-coordination mode of a reduced TEMPO radical as a monoanionic ligand.[7,19] The DFT optimized structure of **1*t*** was found to be C_{2h} symmetric and has structural parameters in reasonable agreement with those of the X-ray crystal structure (Table 1). The metal−ligand bonds are slightly longer than experiment (0.046 for r_{e-Ni-O} and 0.037 Å for r_{e-Ni-N}). Typical of DFT results, intraligand bonding (C−C, N−O TEMPO bonds) are shorter than the X-ray crystal structure parameters of **1*t***.

Table 1. Geometric Parameters of Compound 1 Using the PBE Level of Theory

Ni(η^2-TEMPO)$_2$	Theory **1*t***	Expt. **1**
Ni−O, r_e	1.8870 Å	1.8404 Å
Ni−N, r_e	1.9733 Å	1.9360 Å
N−O TEMPO r_e	1.3882 Å	1.4136 Å
N−Ni−O angle	41.89°	43.88°
O−N−C angle	112.13°	110.83°
C−N−C angle	116.46°	116.59°
free TEMPO radical N−O, r_e	1.2798 Å	1.283 Å[a]
free TEMPO anion N−O, r_e	1.3966 Å	

[a]Data taken from ref 19.

The "*cis*" complex with C_2 point group symmetry has also been theoretically determined (**1*c***; see Scheme 2). Scheme 2 also shows 2D illustrations and a simplified rendition of the 2D structural skeleton of **1** that will be used throughout further schemes. In the *cis* structure, the Ni−O bond is shortened, while the Ni−N bond is elongated. For all substituted complexes (vida infra) as well as complex **1**, only a single isomer has been isolated and characterized experimentally. Cartesian coordinates of the unobserved isomers (complexes **1*c***, **2*t***, **3*t***, **4*c***, **5*t***, **6*t***, **8*t***, **9*ct***, and **9*tt***) are presented in the Supporting Information.

Two monoanionic η^2-TEMPO ligands can each serve as 2 e$^-$ donors giving the Ni atom a 16-electron configuration and a

dx.doi.org/10.1021/ic401296f | *Inorg. Chem.* 2013, 52, 13882−13893

Scheme 2. Structure of 1*c* and 1*t*[a]

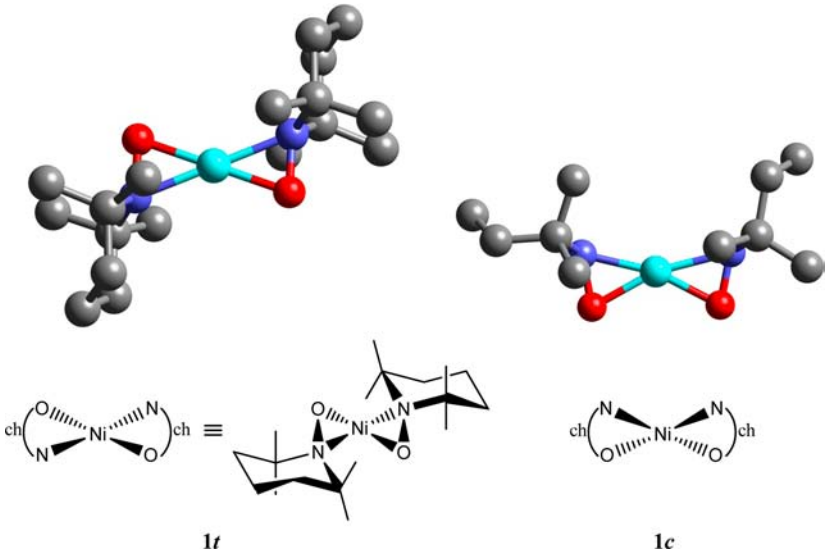

[a]Hydrogen atoms omitted for clarity.

formal oxidation state of 2+ (d^8). ^{1}H NMR study of **1** confirmed that the solid-state η^2-binding mode persists in solution, displaying magnetically inequivalent methyl groups on the ring as two distinct sets exist on differing sides of the N−O bonds. Even at much higher and lower temperatures these Ni−O−N metallacycles appear to be stable on the NMR time scale, as little change was found in the ^{1}H NMR spectrum from −80 °C to 90 °C in toluene-d_8.

Compound **1** reacts with *tert*-butyl isocyanide, CN^{t}Bu, at room temperature to give the complex Ni(η^2-TEMPO)(η^1-TEMPO)(κ^1-CN^{t}Bu) (**2**) in 90% yield. Its structure in the solid state is shown in Figure 2.

As can be seen in Scheme 1 and Figure 2, compound **2** has a distorted planar structure, but importantly, the complex has isomerized to a *cis* form and one of the η^2-TEMPO ligands in the starting complex **1** has adopted an η^1-bonding mode. The electron count around nickel remains at 16 with the CN^{t}Bu and η^1-TEMPO groups each, acting as two electron donors. The two TEMPO ligands remain reduced in **2**, giving a formal oxidation state of 2+ on the nickel. The computed geometric parameters of *cis*-Ni(η^2-TEMPO)(η^1-TEMPO)(κ^1-CN^{t}Bu) (**2*c***) are also in reasonable agreement with those of the X-ray crystal structure (see Table S4 in the Supporting Information). Both computed species also have a pseudo square-planar geometry. Computations were attempted in order to rule out the possibility of a square pyramidal Ni(η^2-TEMPO)$_2$(κ^1-CN^{t}Bu) complex,[7] and all attempts collapsed to **2*t*** or **2*c***.

When 1 equiv of phenylacetylene was added to a hexane solution of **1**, a color change from purple to light red occurred over a period of less than 1 h. The reaction is almost instantaneous at 68 °C in refluxing hexane solvent. The removal of volatiles in vacuo and crystallization from diethyl ether resulted in light red bars of the phenylacetylide complex Ni(η^2-TEMPO)(κ^1-TEMPOH)(κ^1-CCPh) (**3**) in 73% yield. Single-crystal X-ray crystallographic analysis indicated the distorted square planar structure for **3**, as shown in Figure 3.

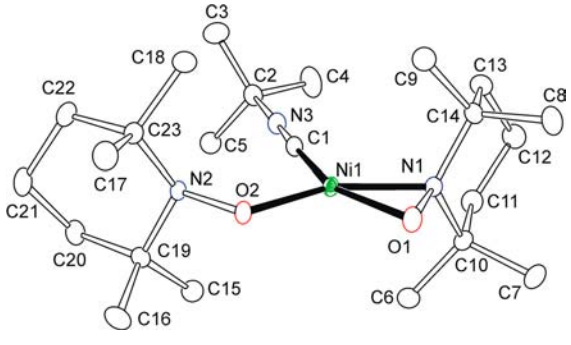

Figure 2. An ORTEP of the molecular structure of **2**, showing 50% thermal ellipsoid probability. Selected bond distances and angles are as follows: Ni1−O1 = 1.8796(7) Å, Ni1−N1 = 1.8801(8) Å, Ni1−O2 = 1.8378(7) Å, Ni1−C1 = 1.8210(10) Å, N1−O1 = 1.3851(10) Å, N2−O2 = 1.4354(10) Å, and C1−N3 = 1.1544(13) Å; N1−Ni1−O1 = 43.23(3)°, O1−Ni1−C1 = 153.50(4)°, C1−Ni1−O2 = 100.59(4)°, N1−Ni1−C1 = 110.27(4)°, O1−Ni1−O2 = 105.90(3)°, N2−O2−Ni1 = 115.02(5)°, Ni1−N1−O1 = 68.37(4)°, and Ni1−O1−N1 = 68.40(4)°.

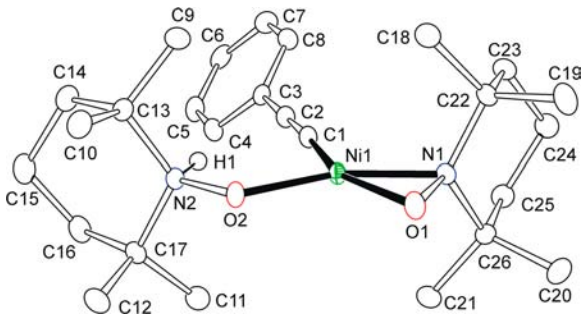

Figure 3. An ORTEP of the molecular structure of **3**, showing 50% thermal ellipsoid probability. Selected bond distances and angles are as follows: Ni1−O1 = 1.8868(7) Å, Ni1−N1 = 1.8608(8) Å, Ni1−O2 = 1.8927(7) Å, Ni1−C1 = 1.8648(10) Å, N1−O1 = 1.3869(10) Å, N2−O2 = 1.4048(10) Å, and C1−C2 = 1.2205(14) Å; N1−Ni1−O1 = 43.43(3)°, O1−N1−C22 = 112.57(7)°, O1−N1−C26 = 112.92(7)°, C22−N1−C26 = 118.21(7)°, O2−N2−C13 = 110.87(7)°, O2−N2−C17 = 110.52(7)°, C13−N2−C17 = 118.06(7)°.

dx.doi.org/10.1021/ic401296f | *Inorg. Chem.* 2013, 52, 13882−13893

The fate of the H atom from the phenylacetylene molecule was monitored by ^{1}H NMR, which indicated a peak at 7.62 ppm with an appropriate integration of ^{1}H. Based on the crystal structure data collected at 100 K, the H atom was located and refined satisfactorily on the N2 atom, as shown in Figure 3. The location of the H atom on nitrogen was confirmed by 2D [^{1}H, ^{15}N] HSQC NMR, which showed a direct correlation between atoms N2 and H1 with an observed $^1J(^{15}N-H)$ coupling constant of 78 Hz (see Figure S2 in the Supporting Information).[20] The reaction of **1** with phenylacetylene-d_1 (99%) gave the complex **3**-d_1 and its ^{1}H NMR spectrum showed all the appropriate resonances for **3** (see Figure S4 in the Supporting Information), with the exception of the peak at 7.62 ppm, which was almost completely absent. Compound **3** remains a 16-electron Ni(II) complex, with the κ^1-TEMPOH ligand acting as a 2-electron donor neutral ligand. The κ^1-TEMPOH ligand can be viewed as the N-protonated isomer of free neutral TEMPOH (where H is bonded to O). This type of bonding mode for κ^1-TEMPOH is quite rare in transition-metal complexes, and there are only a few other crystallographically characterized examples.[6c,21] Interestingly, the structure of **3** is also *cis*-disposed, compared to the unsubstituted complex **1**. Computed geometries of **3c** (see Table S5 in the Supporting Information) show excellent structural agreement with the experimental crystal structure due to an elongated Ni−O η^2-TEMPO bond and a much shorter Ni−N η^2-TEMPO optimized bond length. In free TEMPO, the N−O bond length is 1.283(9) Å,[19] while, once coordinated, the N−O bond length is elongated (by more than ∼0.1 Å), as expected for a reduced monoanionic ligand, along with a pyramidal geometry about the nitroxyl N atom. It is interesting to note that, in both compounds **2** and **3** (along with the other subsequent complexes), the side-bound η^2-TEMPO always has a shorter N−O bond than the end-bound η^1-TEMPO. These results suggest the η^1-TEMPO ligand is more anionic than the η^2-TEMPO ligand, perhaps depopulating a N−O antibonding orbital in the η^2 case, with the net result that the Ni center donates more electrons to η^1-TEMPO.

The reaction of **1** with a 1:1 mixture of PhCCH and PhCCD in toluene-d_8 solvent at room temperature was followed by ^{1}H NMR. Integration of the resonances of the product showed an ∼50:50 ratio for the formation of products **3** and **3**-d_1, indicating that there was no discernible difference in the rates of formation between products **3** and **3**-d_1. The reaction was also monitored by ^{2}H{^{1}H} NMR using toluene solvent and appropriate integration of the singlet deuterium resonances in the starting PhCCD versus the product N−D resonances in **3**-d_1 also showed an ∼50:50 ratio. This reaction was also repeated using a 6:6 mixture of PhCCH and PhCCD, to give the same product ratio (see Figures S5 and S6 in the Supporting Information). This result is interpreted as being consistent with an addition mechanism in which deprotonation of the C−H or C−D bond is not rate-determining, in keeping with computational results discussed in the Supporting Information.

Compound **1** reacts with other 2-electron nitrogen donor ligands such as pyridine to yield the complex Ni(η^2-TEMPO)(η^1-TEMPO)(κ^1-NC_5H_5) (**4**) in 95% yield at room temperature. Compound **4** also contains an η^1-TEMPO ligand and the orientation of the pyridine ring is coplanar with the distorted square planar geometry around nickel (see Figure 4). Unlike the previous substituted complexes, the pyridine adduct is the only one observed in this study that retains the *trans*-disposition of the original complex.

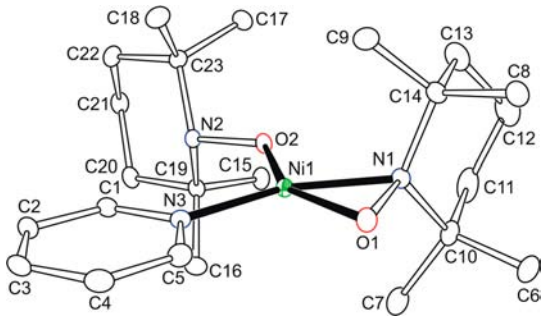

Figure 4. An ORTEP of the molecular structure of **4**, showing 50% thermal ellipsoid probability. Selected bond distances and angles are as follows: Ni1−O2 = 1.8407(10) Å, Ni1−N1 = 1.9063(12) Å, Ni1−O1 = 1.8690(10) Å, Ni1−N3 = 1.9032(12) Å, N1−O1 = 1.3946(15) Å, and N2−O2 = 1.4308(15) Å; O2−Ni1−O1 = 148.36(4)°, O2−Ni1−N3 = 108.55(5)°, O1−Ni1−N3 = 103.08(5)°, O2−Ni1−N1 = 105.04(5)°, O1−Ni1−N1 = 43.34(5)°, N3−Ni1−N1 = 146.23(5)°, O1−N1−Ni1 = 66.91(6)°, O1−N1−C14 = 112.02(11)°, O1−N1−C10 = 112.71(11)°, and O2−N2−C23 = 107.48(10)°.

When compound **4** was dissolved in any noncoordinating solvent such as toluene or benzene, it was immediately converted back to **1**, liberating free pyridine. The ^{1}H NMR spectrum of **4** in pyridine-d_5 solvent did not show the resonance of the pyridine ligand, because it was rapidly exchanged with pyridine-d_5 from the solvent. A series of experiments for the addition of excess amounts of pyridine (49−294 equiv) to **1**, were monitored by ^{1}H NMR (see Figure S7 in the Supporting Information), which did not show complete conversion of starting material (**1**) to **4**. Using a rough estimate of ∼80% conversion to **4** in pure pyridine solvent, a K_{eq} value of 0.33 was estimated. This result suggests that binding of pyridine is very poor (in agreement with the computational results, vida infra). Furthermore, the ^{1}H NMR spectrum at room temperature showed broad, overlapping peaks indicative of fluxional processes associated with the TEMPO ligand. Variable-temperature ^{1}H NMR spectra in the range of −40° to 105 °C (see Figure S3 in the Supporting Information) did not reveal a static spectrum that is consistent with the solid state structure of **4**. This fluxional process was also observed in the ^{1}H NMR spectrum of **2** at room temperature. Variable-temperature ^{1}H NMR spectra in the range of 25°−90 °C resulted in some sharpening of the peaks. However, as shown in Figure S1 in the Supporting Information, some broadening remained, even at that temperature. At temperatures above 90 °C, **2** decomposes. It is clear that some broadening and exchange occur at higher temperatures as well. The exact nature of the fluxional process in **2** and **4** remains unresolved and is beyond the scope of this report. While we are unable to unambiguously assign the dynamical process, work is underway to theoretically determine whether these processes occur due to η^1 to η^2 exchange of the TEMPO ligands in solution or from conformational distortion of TEMPO.

To further test the ability of **1** to react with other terminal alkynes, reactions with acetylene gas and trimethylsilyl acetylene were carried out to afford the acetylide products, Ni(η^2-TEMPO)(κ^1-TEMPOH)(κ^1-CCH) (**5**) and Ni(η^2-TEMPO)(κ^1-TEMPOH)(κ^1-$CCSiMe_3$) (**6**) in yields of 74% and 79%, respectively. ORTEPs for compounds **5** and **6** are shown in Figures 5 and 6, respectively. The structures of both complexes are similar to **3**, where the alkyne moiety is bonded in a κ^1 manner, and one of the TEMPO ligands is a κ^1-

dx.doi.org/10.1021/ic401296f | Inorg. Chem. 2013, 52, 13882−13893

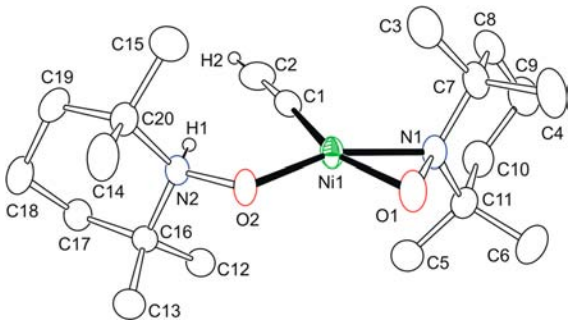

Figure 5. An ORTEP of the molecular structure of **5**, showing 30% thermal ellipsoid probability. Selected bond distances and angles are as follows: Ni1−O1 = 1.8614(12) Å, Ni1−C1 = 1.8708(15) Å, Ni1−N1 = 1.8750(12) Å, Ni1−O2 = 1.8878(10) Å, N1−O1 = 1.3877(15) Å, N2−O2 = 1.4011(14) Å, and C1−C2 = 1.195(2) Å; O1−Ni1−C1 = 157.23(5)°, O1−Ni1−N1 = 43.60(5)°, C1−Ni1−N1 = 113.66(6)°, O1−Ni1−O2 = 103.17(4)°, C1−Ni1−O2=99.59(5), N1−Ni1−O2 = 146.73(5)°, N1−O1−Ni1 = 68.72(7)°, N2−O2−Ni1 = 117.22(8)°, N2−O2−Ni1 = 117.22(8)°, and O1−N1−Ni1 = 67.68(7)°.

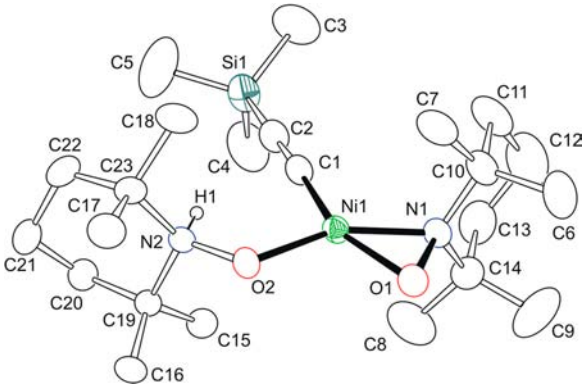

Figure 6. An ORTEP of the molecular structure of **6**, showing 30% thermal ellipsoid probability. Selected bond distances and angles are as follows: Ni1−C1 = 1.860(3) Å, Ni1−N1 = 1.862(2) Å, Ni1−O1 = 1.8701(17) Å, Ni1−O2 = 1.8871(15) Å, C1−C2 = 1.223(4) Å, N1−O1 = 1.388(2) Å, N2−O2 = 1.402(2) Å, and Si1−C2 = 1.806(3) Å; C1−Ni1−N1 = 111.84(9)°, C1−Ni1−O1 = 155.47(9)°, N1−Ni1−O1 = 43.66(7)°, C1−Ni1−O2 = 99.95(9)°, N1−Ni1−O2 = 148.21(7)°, O1−Ni1−O2 = 104.56(7)°, N1−O1−Ni1 = 67.86(11)°, N2−O2−Ni1 = 117.07(12)°, O1−N1−Ni1 = 68.49(11)°.

TEMPOH group. We have been unable to add two alkyne molecules to **1.** Even when excess reagent was used, complexes with only one acetylide group were obtained (see the Dimerization Reactions section below).

For the acetylide complexes **3**, **5**, and **6**, their ^{1}H NMR spectrum show sharp peaks consistent with the solid-state structures. This nonfluxional behavior is because the κ^1-TEMPOH ligand cannot become κ^2 or η^2, since there is now a hydrogen on the nitrogen on one of the TEMPO ligands. The protonation of this nitrogen stops the formation of κ^2-TEMPOH and the η^2-TEMPO ligand remains in an η^2-binding mode, as seen in **2** and **4**.

An experiment was carried out for an exchange reaction to see if **5** could be converted to **3** by the addition of free PhCCH. The conversion does occur at room temperature, but is very slow during which time there is considerable decomposition and provides **3** in only very minor amounts.

Dimerization Reactions. It could be conceived that the reaction of **1** with acetylene gas would also yield a product where another molecule of **1** reacts with **5**, as there is a terminal alkyne moiety available in **5**, to give a structure **7** (Scheme 3).

Scheme 3. Structure of 7[a]

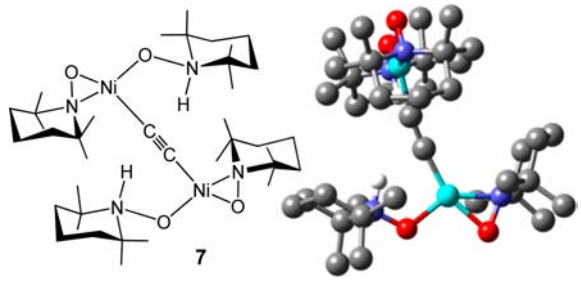

[a]Alkyl hydrogens omitted for clarity.

However, we did not observe this product. This result is explainable in terms of steric crowding limiting accessibility to the already coordinated acetylide ligand. Another possibility could be that the pK_a for the second proton in acetylene is much higher (more basic). While **7** could not be synthesized, we were able to locate this hypothetical structure computationally (see Scheme 3).

Unlike complex **9** (see below), in the computed structure of **7**, one of the Ni(TEMPO)(TEMPOH) moieties is twisted 90° from the other to relieve the pronounced steric repulsion. This complex is not thermodynamically favored over its constituent monomers. The dimerization thermodynamics can be computed in two ways, via the addition of 2 equiv of **1** and 1 equiv of HCCH or via the reaction of **1** and **5**. The computed solution-phase free energy of reaction is quite large and positive for both cases: +5.4 and +9.2 kcal mol^{-1} (see Table 2 and Table S10 in the Supporting Information).

Table 2. Solution-Phase Reaction Free Energies (ΔG_{soln} in kcal mol^{-1}) of Bimetallic Complexes and Relative Free Energies ($\Delta\Delta G_{soln}$ in kcal mol^{-1}) of Isomers of Complex 9

reaction	ΔG_{soln} (kcal mol^{-1})	$\Delta\Delta G_{soln}$ (kcal mol^{-1})
2 equiv **1** + HCCH → **7*cc***	5.4	
5*c* + **1*t*** → **7*cc***	9.2	
9*cc*[a]		0.0
9*ct*		4.1
9*tt*		9.2
2 equiv **1*t*** + HCCPhCCH → **9*cc***	−5.2	
8 + **1*t*** → **9*cc***	−0.8	

[a]Isomer **9*cc*** is arbitrarily set to 0.0 kcal mol^{-1}.

Exploring further efforts to link two Ni(TEMPO)$_2$ molecules, we performed the reaction of **1** with the diyne 1,4-diethynylbenzene. At room temperature, we were able to isolate the complex Ni(η^2-TEMPO)(κ^1-TEMPOH)[κ^1-CC-(C$_6$H$_4$)CCH], **8** in 50% yield. As in the characterized compounds **3**, **5**, and **6**, there is only one acetylide group bonded to the Ni center in **8** (see Figure 7).

When the reaction was carried out with 2 equiv of **1** and 1 equiv of 1,4-diethynylbenzene, we did indeed obtain the

dx.doi.org/10.1021/ic401296f | Inorg. Chem. 2013, 52, 13882−13893

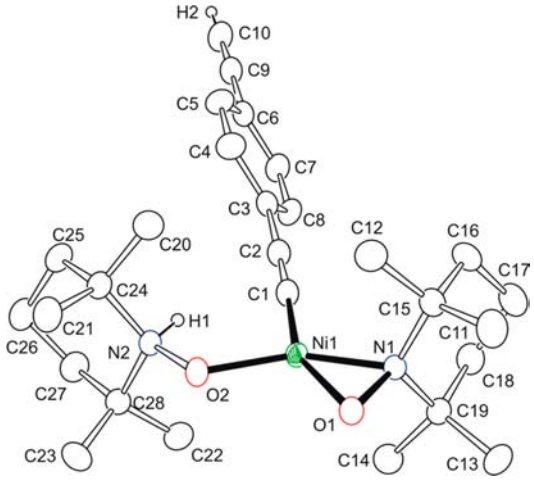

Figure 7. An ORTEP of the molecular structure of **8**, showing 30% thermal ellipsoid probability. Selected bond distances and angles are as follows: Ni1−N1 = 1.8605(9) Å, Ni1−C1 = 1.8748(12) Å, Ni1−O2 = 1.8890(8) Å, Ni1−O1 = 1.8909(8) Å, N1−O1 = 1.3840(11) Å, N2−O2 = 1.4027(12) Å, and C1−C2 = 1.2146(17) Å; N1−Ni1−C1 = 111.22(4)°, N1−Ni1−O2 = 149.15(4)°, C1−Ni1−O2 = 99.43(4)°, N1−Ni1−O1 = 43.29(3)°, C1−Ni1−O1=154.51(4)°, O2−Ni1−O1 = 106.02(3)°, O1−N1−C19 = 113.37(8)°, O1−N1−C15 = 112.25(9)°, O1−N1−Ni1 = 69.52(5)°, N1−O1−Ni1 = 67.19(5)°, and N2−O2−Ni1 = 116.72(6)°.

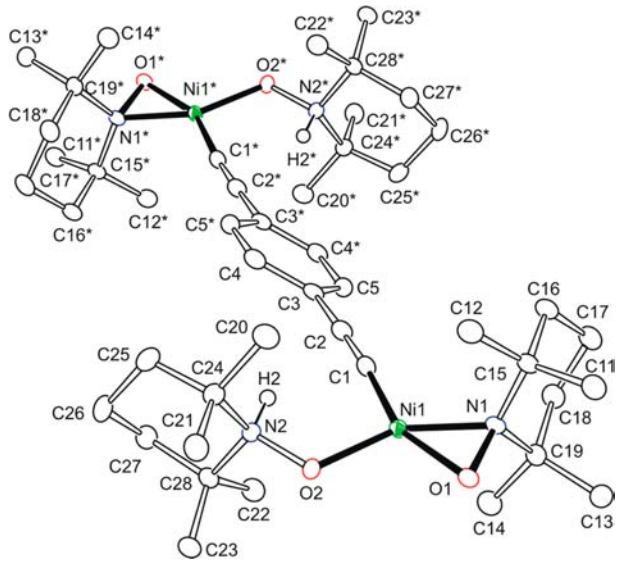

Figure 8. An ORTEP of the molecular structure of **9**, showing 50% thermal ellipsoid probability. Selected bond distances and angles are as follows: Ni1−N1 = 1.8685(16) Å, Ni1−C1 = 1.8582(19) Å, Ni1−O2 = 1.8918(13) Å, Ni1−O1 = 1.8795(13) Å, N1−O1 = 1.3912(19) Å, N2−O2 = 1.4114(19) Å, and C1−C2 = 1.217(3) Å; N1−Ni1−C1 = 112.20(7)°, N1−Ni1−O2 = 149.13(6)°, C1−Ni1−O2 = 98.67(7)°, N1−Ni1−O1 = 43.58(6)°, C1−Ni1−O1 = 155.76(7)°, O2−Ni1−O1 = 105.56(5)°, O1−N1−C19 = 112.62(13)°, O1−N1−C15 = 112.20(14)°, O1−N1−Ni1 = 68.63(8)°, N1−O1−Ni1 = 67.79(8)°, and N2−O2−Ni1 = 117.19(10)°.

complex Ni(η^2-TEMPO)(κ^1-TEMPOH)[κ^1-κ^1-CC(C_6H_4)CC]-Ni(η^2-TEMPO)(κ^1-TEMPOH) (**9**) in 80% yield, where now two Ni(η^2-TEMPO)(κ^1-TEMPOH) groups are linked by a diethynylbenzene group (see Figure 8). Subsequently, compound **9** can also be obtained via the reaction of compound **8** with 1 equiv of **1** at room temperature.

While we have not attempted to model dimerization reaction kinetics or mechanisms, the various isomeric possibilities of **9** have been explored. Three possibilities arise, the *cis*−*cis*, *cis*−*trans*, or *trans*−*trans* isomers, which are labeled **9*cc***, **9*ct***, and **9*tt***, respectively (see Scheme 4).

From Table 2, the **9*cc*** isomer is lowest in solution-phase free energy, by 4.1 and 9.2 kcal mol^{-1}, compared to the **9*ct*** and **9*tt*** isomers, respectively, which is in agreement with the experimental characterization of **9**. The results from Table 2 also confirm that both experimental procedures for producing complex **9**—the addition of 2 equiv of complex **1** to HCC(C_6H_4)CCH, as well as addition of complex **8** to complex **1**—have thermochemically favored reaction free energies.

Thermodynamics and Kinetics of the Possible Products. In each case, except for pyridine, the addition of ligand affords an adduct that contains *cis*-disposed TEMPO ligands. Because of the fact that the majority of the products formed from *trans* Ni(η^2-TEMPO)$_2$ resulted in a *cis* disposition, preliminary computations were initiated for three possible limiting reaction mechanisms, as shown in Scheme 5.

When does this isomerization occur? The first possibility is that isomerization takes place in the initial complex **1*t***, and then **1*c*** undergoes the addition reaction with the alkyne substituent. The second possibility is that the isomerization occurs when the adduct is bound to the complex, but before the hydrogen transfer to the η^1-TEMPO ligand, (i.e., a pathway connecting **11**/**12** to **14**, **16** to **18**, **20** to **22**, or **24** to **26**, shown in Schemes S1−S8 in the Supporting Information). Finally, there is the possibility that *trans*−*cis* isomerization can occur after the hydrogen transfer takes place (in a mechanism between **3*c*** and **3*t***, for example). All of this discussion of *trans*-to-*cis* isomerization is complicated by two factors: (1) the relative energy of the lowest energy **1*c*** isomer is 4.0 kcal mol^{-1} higher than the lowest energy isomer of **1*t*** and (2) astonishingly, the computed NMR spectrum of **1*c*** is very similar to the computed NMR spectrum of **1*t*** (which is in relatively good agreement with the experimentally observed NMR spectrum of **1*t***). Therefore, the very small amount of *cis* isomer produced from raising the temperature would only slightly alter the peak integrations. (See the Supporting Information for further discussion of these points.)

Proposed pathways for the addition reactions of the *tert*-butyl isocyanide and pyridine are presented in the following section. First, transition states corresponding to the addition of the CN^{t}Bu ligand to the *cis* and *trans* form of **1** have been computed and proceed via a simple association reaction. Both the *cis* and *trans* transition states (**TS-2*c*** and **TS-2*t***, respectively) possess an imaginary mode with Ni−N−O ring opening coupled to ligand addition. The PBE transition state of the *trans* structure (Scheme 6) has a Ni−N bond distance of 2.427 Å, versus 2.807 Å for the *cis* structure.

From Scheme 6, it is evident that **2*c*** and **2*t*** are nearly isoenergetic. In the solution-phase computations, the experimentally observed **2*c*** isomer is only 0.1 kcal mol^{-1} lower in free energy. Theory shows the experimentally observed isomer being slightly favored thermodynamically, but disfavored kinetically (the $\Delta G^{\ddagger}$ value of **TS-2*c*** is 15.1 kcal mol^{-1}, versus **TS-2*t*** with a $\Delta G^{\ddagger}$ value of 13.8 kcal mol^{-1}). Among the complexes considered in this paper, the **2*c***/**2*t*** pair shows the closest relative free energies, in terms of both kinetics and thermodynamics. However, attempts to force crystallization of the **2*t*** isomer under a variety of experimental conditions

dx.doi.org/10.1021/ic401296f | *Inorg. Chem.* 2013, 52, 13882−13893

Scheme 4

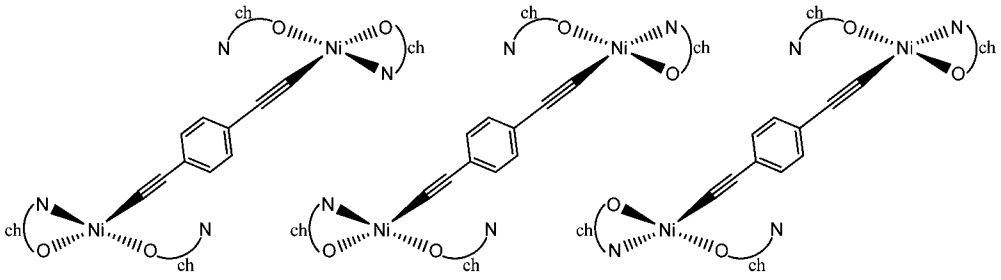

9cc **9ct** **9tt**

Scheme 5. Isomerization Possibilities of Addition Reactions

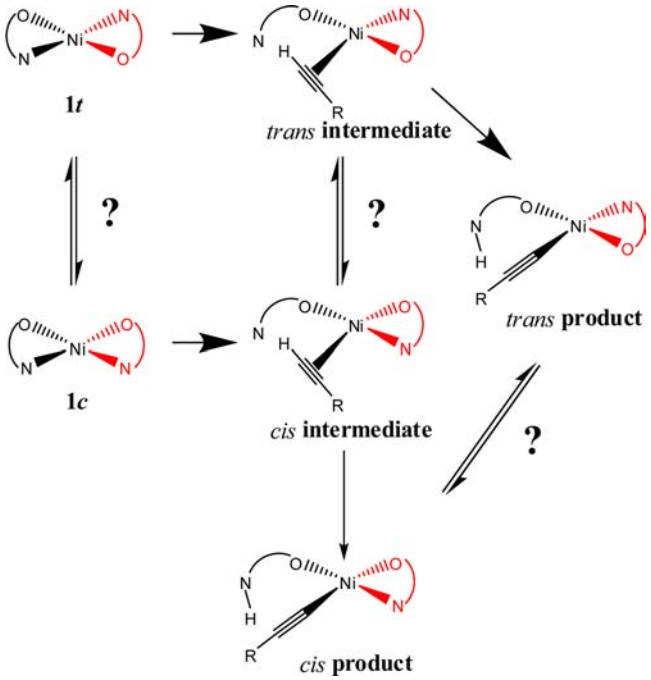

(variation of temperature and solvents) were unsuccessful and only resulted in formation of **2c** crystals.

In Scheme 7, the thermodynamics of pyridine addition to complex **1t** to form complex **4t** is shown. **4t** is the least thermodynamically stable of the various adducts that have been considered in this study, because it is the only one where the experimentally characterized structure has a computed positive free energy of reaction (+2.1 kcal mol^{-1}, which corresponds to a K_{eq} value of 0.0288). **4** is also the only adduct where the *trans* isomer has been isolated experimentally. The computed lower stability matches with the experimentally observed short lifetime/fast exchange in pyridine solvent and low-temperature decomposition of **4t**. From the experimental NMR measurements, the value of K_{eq} was determined to be ~0.33 (corresponds to a ΔG of 0.65 kcal mol^{-1}). This K_{eq} value is slightly greater than the value obtained from the solution-phase computations (0.0288).

The addition reactions for other ligands (acetylene, 1,4-diethynylbenzene, and trimethylsilyl acetylene) were also studied, but the results are less convincing. For all cases (including the results provided in the Supporting Information), the computed thermodynamics for the addition reactions are consistent with the experimentally observed product isomer (see Table 3 and Table S7 in the Supporting Information). However, in each case, the computational results indicate that the *trans* complex is the kinetic product. In the case of pyridine addition, the *trans* product is both the kinetic and thermodynamic product. In all other cases, experiments to isolate the kinetic product were not successful. The inclusion of the loss of the gas-phase entropic contribution may not accurately reflect the smaller loss of translational entropy from the solvated ligand molecule, which is necessarily already in solution. Both the gas phase and PCM solution computations appear to overestimate the loss of translation entropy when an adduct is formed from infinitely separated reactants. One could include a reduction in the loss of translational entropy (from gas phase to solution phase), but without further kinetic measurements (that are beyond the scope of the current contribution) against which to measure, an arbitrary scaling of this translational entropic contribution does not provide intellectually satisfying results.

SUMMARY AND CONCLUSIONS

A summary of the reactions of the title complex **1** described in this report is shown in Scheme 1. Bifunctional cooperativity between the hemilabile TEMPO ligand and the Ni center in **1** has been demonstrated in its reactivity with organic substrates at room temperature. The addition of terminal alkynes to yield the respective acetylide products is rare, with the N atom on the TEMPO ligand acting as a base to deprotonate the alkyne. Furthermore, the reaction with terminal alkynes is not restricted to phenylacetylene, but general for alkyne molecules. Complex **9** is a good example that demonstrates that subsequent proton transfer can occur to link two Ni(η^2-TEMPO)(κ^1-TEMPOH) groups, in a bridging dinuclear complex.

Density functional theory (DFT) has been employed to study the structural and thermochemical properties of the molecules shown in Scheme 1. Computed solution-phase relative free energies of the various characterized Ni-centered complexes are in agreement with the experimentally observed isomers. However, rate-limiting transition states of the addition reactions suggest that, in all cases except for the initial Ni(η^2-TEMPO)$_2$ complex **1** and the product formed via the addition of pyridine (**4t**), the experimentally observed isomer is always kinetically disfavored. The mechanism by which the *trans* complex **1** isomerizes to the various *cis* product complexes upon substrate addition is still not completely understood. Further experimental and computational work will be performed in tandem to explore the fascinating conformational complexity of the isomerization reactions. Both theory and experiment also validate the formation of the bimetallic complex **9** (two C−H bond activations of 1,4-diethynylben-

dx.doi.org/10.1021/ic401296f | *Inorg. Chem.* 2013, 52, 13882−13893

Scheme 6. Addition of CN^{t}Bu

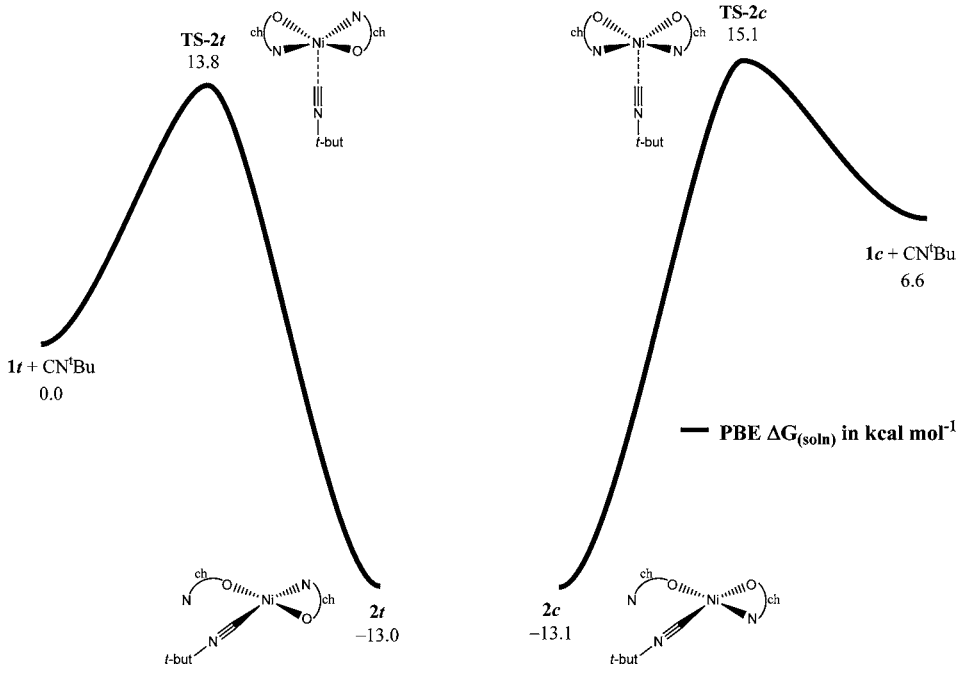

Scheme 7. Addition of Pyridine

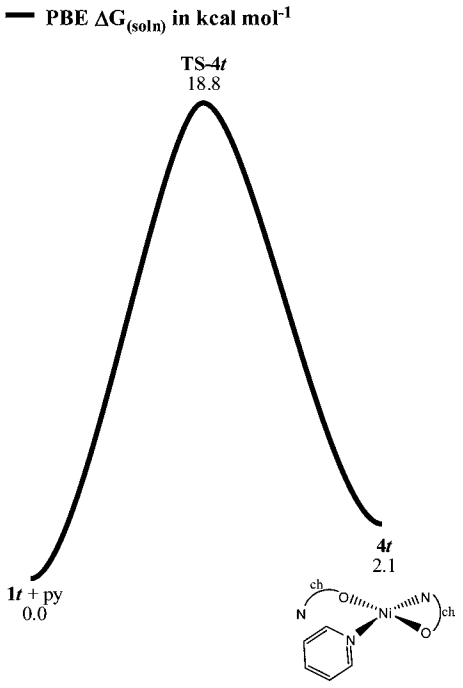

zene) and are correspondingly in agreement that the proposed bimetallic complex **7** (two C−H bond activations of acetylene) will be too sterically crowded to exist under the same experimental conditions used to isolate complexes **1**−**6**, **8**, and **9**.

The reactions presented in this report are facile under mild conditions. The brief survey of reactions that are contained within present a good start. Further studies in the realm of homogeneous catalysis, targeting small molecule and C−H activation, carbon−carbon coupling, and oxygen atom transfer, are planned.

Table 3. Theoretical PBE Solution-Phase Reaction Free Energies (ΔG_{soln}) for the Addition of All Ligands to Complex 1[a]

reaction	reaction free energy, ΔG_{soln} (kcal mol^{-1})
1*t*	**0.0**
1*c*	4.0[b]
1*t* + CN^{t}Bu → **2*t***	−13.0
1*t* + CN^{t}Bu → **2*c***	**−13.1**
1*t* + PhCCH → **3*t***	1.2
1*t* + PhCCH → **3*c***	**−3.3**
1t + py → **4t**	**2.1**
1t + py → **4c**	5.6
1t + HCCH → **5t**	−2.5
1t + HCCH → **5c**	**−3.8**
1*t* + HCCSi(CH$_3$)$_3$ → **6*t***	−0.1
1t + HCCSi(CH$_3$)$_3$ → **6c**	**−4.2**
1*t* + HCCPhCCH → **8*t***	−0.8
1*t* + HCCPhCCH → **8*c***	**−4.4**

[a]Further computational results for the gas-phase thermodynamics and gas-phase and solution-phase kinetics are included in the Supporting Information. Included in the first rows are the relative energies of the *trans* and *cis* isomers of complex **1**. The reaction free energy of the experimentally observed isomer is shown in bold text. [b]The relative free energy of **1*c*** refers to the lowest energy conformer. The conformer that directly reacts to form the various addition products is slightly higher in free energy (ΔG_{soln} = 6.6 kcal mol^{-1}); and this relative free energy is used along the reaction mechanisms shown in Schemes 6, S2, S4, S6, S8, and S9.

dx.doi.org/10.1021/ic401296f | *Inorg. Chem.* 2013, 52, 13882−13893

■ ASSOCIATED CONTENT

Supporting Information

Crystallographic data of **1**, **2**, **3**, **4**, **5**, **6**, **8**, and **9** (in CIF format), various experimental and computational NMR spectra, computed addition reactions with postulated mechanisms for the formation of **3*t*/3*c***, **5*t*/5*c***, **6*t*/6*c***, and **8*t*/8*c***, further computational results, and detailed geometric parameters of all computed stationary points. This material is available free of charge via the Internet at http://pubs.acs.org.

■ AUTHOR INFORMATION

Corresponding Authors

*E-mail: cewebstr@memphis.edu (C.E.W.).
*E-mail: captain@miami.edu (B.C.).

Notes

The authors declare no competing financial interest.

■ ACKNOWLEDGMENTS

B.C. gratefully acknowledges support by the National Science Foundation (Nos. CHE-1300206 and CHE-0946858 - funds toward the purchase of LC-ESI-MS). In addition, Christoph Fahrni (Georgia Tech) is thanked for helpful discussions. C.E.W. acknowledges the National Science Foundation (Nos. CHE-0955723 and CHE-0911528) for financial support. C.E.W. and N.J.D. thank the University of Memphis High Performance Computing Facility and Computational Research on Materials Institute (CROMIUM) for computing support.

■ REFERENCES

(1) (a) Ciriminna, R.; Pagliaro, M. *Org. Process Res. Dev.* **2010**, *14*, 245−251. (b) Lebedev, O. L.; Kazarnovskii, S. N. *Zh. Obshch. Khim.* **1960**, *30*, 1631−1635.

(2) (a) Georges, M. K.; Lukkarila, J. L.; Szkurhan, A. R. *Macromolecules* **2004**, *37*, 1297−1303. (b) Maehata, H.; Buragina, C.; Cunningham, M.; Keoshkerian, B. *Macromolecules* **2007**, *40*, 7126−7131. (c) Hawker, C. J. *Acc. Chem. Res.* **1997**, *30*, 373−382. (d) Benoit, D.; Chaplinski, V.; Braslau, R.; Hawker, C. J. *J. Am. Chem. Soc.* **1999**, *121*, 3904−3920.

(3) (a) Hu, S.; Gao, W.; Kumar, R.; Gross, R. A.; Gu, Q.-M.; Cheng, H. N. In *Biocatalysis in Polymer Science*; Gross, R. A., Cheng, H. N., Eds.; ACS Symposium Series 840; American Chemical Society: Washington, DC, 2002; Chapter 21, pp 253−264. (b) Michaud, A.; Gingras, G.; Morin, M.; Beland, F.; Cirimimna, R.; Avnir, D.; Pagliaro, M. *Org. Process Res. Dev.* **2007**, *11*, 766−768. (c) Bordenave, N.; Grelier, S.; Coma, V. *Biomacromolecules* **2008**, *9*, 2377−2382. (d) deNooy, A. E. J.; Besemer, A. C.; van Bekkum, H. *Synthesis (Stuttgart)* **1996**, 1153−1174. (e) Sheldon, R. A.; Arends, I. W. C. E. *Adv. Synth. Catal.* **2004**, *346*, 1051−1071. (f) Recupero, F.; Punta, C. *Chem. Rev.* **2007**, *107*, 3800−3842. (g) Semmelhack, M. F.; Schmid, C. R.; Cortes, D. A. *Tetrahedron Lett.* **1986**, *27*, 1119−1122. (h) Laugier, J.; Latour, J.-M.; Caneshi, A.; Rey, P. *Inorg. Chem.* **1991**, *30*, 4474−4477. (i) Gamez, P.; Arends, I.; Reedijk, J.; Sheldon, R. *Chem. Commun.* **2003**, 2414−2415. (j) Cheng, L.; Wang, J.; Wang, M.; Wu, Z. *Inorg. Chem.* **2010**, *49*, 9392−9399.

(4) (a) Keana, J. F. W. *Chem. Rev.* **1978**, *78*, 37−64. (b) Borbat, P. P.; Costa-Filho, A. J.; Earle, K. A.; Moscicki, J. K.; Freed, J. H. *Science* **2001**, *291*, 266−269. (c) Chen, J. Y.-C.; Jayaraj, N.; Jockusch, S.; Ottaviani, M. F.; Ramamurthy, V.; Turro, N. J. *J. Am. Chem. Soc.* **2008**, *130*, 7206−7207. (d) Jayaraj, N.; Porel, M.; Ottaviani, M. F.; Maddipatla, M. V. S. N.; Modelli, A.; Da Silva, J. P.; Bhogala, B. R.; Captain, B.; Jockusch, S.; Turro, N. J.; Ramamurthy, V. *Langmuir* **2009**, *25*, 13820−13832. (e) Yi, S.; Captain, B.; Ottaviani, M. F.; Kaifer, A. E. *Langmuir* **2011**, *27*, 5624−5632. (f) Dane, E. L.; Maly, T.; Debelouchina, G. T.; Griffin, R. G.; Swagger, T. M. *Org. Lett.* **2009**, *11*, 1871−1874.

(5) (a) Pervukhina, N. V.; Romanenko, G. V.; Podberezskaya, N. V. *J. Struct. Chem.* **1994**, *35*, 367−390. (b) Dong, T.-Y.; Hendrickson, D. N.; Felthouse, T. R.; Shieh, H.-S. *J. Am. Chem. Soc.* **1984**, *106*, 5373−5375. (c) Felthouse, T.; Dong, T.-Y.; Hendrickson, D.; Shieh, H.-S.; Thompson, M. R. *J. Am. Chem. Soc.* **1986**, *108*, 8201−8214. (d) Dickman, M. H.; Porter, L. C.; Doedens, R. J. *Inorg. Chem.* **1986**, *25*, 2595−2599. (e) Caneschi, A.; Grand, A.; Laugier, J.; Rey, P.; Subra, R. *J. Am. Chem. Soc.* **1988**, *110*, 2307−2309. (f) Jaitner, P.; Huber, W. *J. Organomet. Chem.* **1983**, *259*, C1−5. (g) Jaitner, P.; Huber, W. *J. Organomet. Chem.* **1986**, *311*, 379−385. (h) Jaitner, P.; Huber, W. *Z. Anorg. Allg. Chem.* **1986**, *538*, 53−60. (i) Dickman, M.; Doedens, R. *Inorg. Chem.* **1982**, *21*, 682−684. (j) Mindiola, D. J.; Waterman, R.; Jenkins, D. M.; Hillhouse, G. L. *Inorg. Chim. Acta* **2003**, *345*, 299−308. (k) Ito, M.; Matsumoto, T.; Tatsumi, K. *Inorg. Chem.* **2009**, *48*, 2215−2223. (l) Zhu, Z.; Fettinger, J. C.; Olmstead, M. M.; Powers, P. P. *Organometallics* **2009**, *28*, 2091−2095. (m) Evans, W. J.; Perotti, J. M.; Doedens, R. J.; Ziller, J. W. *Chem. Commun.* **2001**, 2326−2327. (n) Mahanthappa, M. K.; Huang, K.-W.; Cole, A. P.; Waymouth, R. M. *Chem. Commun.* **2002**, 502−503. (o) Huang, K.-W.; Cole, A. P.; Musgrave, C. B.; Waymouth, R. M. *J. Am. Chem. Soc.* **2005**, *127*, 3807−3816.

(6) (a) Hoover, J. M.; Stahl, S. S. *J. Am. Chem. Soc.* **2011**, *133*, 16901−16910. (b) Hoover, J. M.; Ryland, B. L.; Stahl, S. S. *J. Am. Chem. Soc.* **2013**, *135*, 2357−2367. (c) Scepaniak, J. J.; Wright, A. M.; Lewis, R. A.; Wu, G.; Hayton, T. W. *J. Am. Chem. Soc.* **2012**, *134*, 19350−19353. (d) Wright, A. M.; Zaman, H. T.; Wu, G.; Hayton, T. W. *Inorg. Chem.* **2013**, *52*, 3207−3216. (e) Belanzoni, P.; Michel, C.; Baerends, E. J. *Inorg. Chem.* **2011**, *50*, 11896−11904. (f) Ragagnin, G.; Betzemeier, B.; Quici, S.; Knochel, P. *Tetrahedron* **2002**, *58*, 3985−3991. (g) Lu, Z.; Costa, J. S.; Roubeau, O.; Mutikainen, I.; Turpeinen, U.; Teat, S. J.; Gamez, P.; Reedijk, J. *Dalton Trans.* **2008**, 3567−3573. (h) Smith, J. M.; Mayberry, D. E.; Margarit, C. G.; Sutter, J.; Wang, H.; Meyer, K.; Bontchev, R. P. *J. Am. Chem. Soc.* **2012**, *134*, 6516−6519. (i) Lippert, C. A.; Soper, J. D. *Inorg. Chem.* **2010**, *49*, 3682−3684. (j) Lomont, J. P.; Nguyen, S. C.; Harris, C. B. *J. Am. Chem. Soc.* **2013**, *135*, 11266−11273.

(7) Isrow, D.; Captain, B. *Inorg. Chem.* **2011**, *50*, 5864−5866.

(8) *Apex2 Version 2.2-0 and SAINT+ Version 7.46A*; Bruker Analytical X-ray Systems, Inc.: Madison, WI, 2007.

(9) (a) Sheldrick, G. M. *SHELXTL Version 6.1*; Bruker Analytical X-ray Systems, Inc.: Madison, WI, 2000. (b) Sheldrick, G. M. *Acta Crystallogr., Sect. A: Found. Crystallogr.* **2008**, *A64*, 112−122.

(10) Frisch, M. J. et al. *Gaussian 09, Rev. B.01*; Gaussian, Inc.: Wallingford, CT, 2009.

(11) Parr, R. G.; Yang, W. *Density Functional Theory of Atoms and Molecules*; Oxford University Press: New York, 1989.

(12) (a) Becke, A. D. *J. Chem. Phys.* **1993**, *98*, 5648−5652. (b) Lee, C.; Yang, W.; Parr, R. G. *Phys. Rev. B* **1988**, *37*, 785−789.

(13) (a) Perdew, P. J.; Burke, K.; Ernzerhof, M. *Phys. Rev. Lett.* **1996**, *77*, 3865−3868. (b) Perdew, P. J.; Burke, K.; Ernzerhof, M. *Phys. Rev. Lett.* **1997**, *78*, 1396.

(14) Default pruned fine grids (75 radial shells, 302 angular points) for energies and default pruned course grids for gradients and Hessians (35 radial shells, 110 angular points).

(15) (a) Hay, P. J.; Wadt, W. R. *J. Chem. Phys.* **1985**, *82*, 299−310. (b) Wadt, W. R.; Hay, P. J. *J. Chem. Phys.* **1985**, *82*, 284−298.

(16) Couty, M.; Hall, M. B. *J. Comput. Chem.* **1996**, *17*, 1359−1370.

(17) Hariharan, P. C.; Pople, J. A. *Theor. Chim Acta* **1973**, *28*, 213−222. The 6-31G(d′) basis set has the d polarization functions for C, N, and O taken from the 6-311G(d) basis set, instead of the original arbitrarily assigned value of 0.8 used in the 6-31G(d) basis set. Foresman, J. B.; Frisch, Æ. *Exploring Chemistry with Electronic Structure Methods*, 2nd Ed.; Gaussian, Inc.: Pittsburgh, PA; 1996, p 110.

(18) Marenich, A. V.; Cramer, C. J.; Truhlar, D. G. *J. Phys. Chem. B* **2009**, *113*, 6378−6396.

(19) Capiomont, P. A.; Lajzerowicz-Bonneteau, J. *Acta Crystallogr., Sect. B: Crystallogr. Cryst. Chem.* **1974**, *30*, 2160−2166.

(20) (a) Bax, A.; Griffey, R. H.; Hawkins, B. L. *J. Magn. Reson.* **1983**, *55*, 301−315. (b) Carlton, L.; Staskun, B.; van Es, T. *Magn. Reson.*

Chem. **2006**, *44*, 510−514. (c) Chaudhry, A. F.; Mandal, S.; Hardcastle, K. I.; Fahrni, C. *Chem. Sci.* **2011**, *2*, 1016−1024.
(21) (a) Hetterscheid, D. G. H.; Kaiser, J.; Reijerese, E.; Peters, T. P. J.; Thewissen, S.; Blok, A. N. J.; Smits, J. M. M.; de Gelder, R.; de Bruin, B. *J. Am. Chem. Soc.* **2005**, *127*, 1895−1905. (b) Ahlers, C.; Dickman, M. H. *Inorg. Chem.* **1998**, *37*, 6337−6340.